

Effect of carbon vacancies on structural and mechanical properties of stable zirconium carbides: A first principles study

Congwei Xie^{a, b, *}, Artem R. Oganov^{c, d, a, e †}, Duan Li^{b, a}, Tekalign Terfa Debela^{a, b},
Ning Liu^{b, a}, Dong Dong^{a, b}, Qingfeng Zeng^{b, a}, Ali Nasir Chaudhry^{b, a}

^aInternational Center for Materials Discovery, School of Materials Science and Engineering, Northwestern Polytechnical University, Xi'an, Shaanxi 710072, PR China

^bScience and Technology on Thermostructural Composite Materials Laboratory, School of Materials Science and Engineering, Northwestern Polytechnical University, Xi'an, Shaanxi 710072, PR China

^cSkolkovo Institute of Science and Technology, 5 Nobel street, Skolkovo 143025, Russia

^dMoscow Institute of Physics and Technology, 9 Institutskiy Lane, Dolgoprudny City, Moscow Region 141700, Russia

^eDepartment of Geosciences and Center for Materials by Design, Stony Brook University, Stony Brook, New York 11794, USA

* xiecw1021@mail.nwpu.edu.cn

† artem.oganov@stonybrook.edu

Abstract

By using evolutionary algorithm USPEX, we have predicted a number of stable zirconium carbides. In addition to the well-known rocksalt-type stoichiometric ZrC ($Fm\bar{3}m$), present prediction also identifies five stable substoichiometric zirconium carbides adopting rocksalt-type structures with ordered carbon vacancies, Zr_8C_7 ($P\bar{1}$), Zr_6C_5 ($C2/m$), Zr_5C_4 ($P\bar{1}$), Zr_3C_2 ($C2/m$), and Zr_2C ($Fd\bar{3}m$). The effects of carbon vacancies on structural and mechanical properties are investigated. We highlight that the distribution of carbon vacancies has significant influence on volume, Pugh's ratio, and hardness. We further propose that hardness can be enhanced by replacing carbon vacancies with suitable elements, in particular nitrogen and oxygen.

Keywords: zirconium carbides; Crystal structure prediction; USPEX; carbon vacancies; hardness

I. Introduction

Transition metal carbides (TMCs) have a broad range of technological applications due to their outstanding hardness, extremely high melting points, good wear and corrosion resistance, and excellent thermal conductivity^[1-6]. Structures of most TMCs are based on close packing of metal atoms, with C atoms occupying octahedral voids. In substoichiometric TMCs, not all octahedral voids are occupied by C atoms. Because of carbon vacancies, properties of substoichiometric TMCs can be very different from their stoichiometric counterparts^[5-9].

In order to understand the properties of substoichiometric TMCs more deeply, we need to clarify the crystal structures of them. Experimentally, structures of substoichiometric TMCs cannot be easily characterized because of similarities to their stoichiometric forms, except the concentration and distribution of carbon vacancies. Due to the weak atomic scattering factor of carbon, the X-ray diffraction patterns between substoichiometric TMCs and their stoichiometric forms are almost undistinguishable^[5,8]. Theoretical methods, in particular the order-parameter functional method^[10-12], and Monte Carlo calculations^[13], in many cases are reliable (e.g., investigations for substoichiometric TMCs Ti_2C , Zr_2C , and V_6C_5 etc.^[5,6,8,14]), but in some cases are questionable (e.g., see examples in Refs. 10-13). The state-of-the-art evolutionary algorithm (EA) for structure prediction, performing global search and implemented in the USPEX code is a promising approach to solve this problem^[15,16]. Using USPEX, many stable substoichiometric TMCs have been found, e.g. in systems Ta-C ^[17], Ti-C ^[18], and Hf-C ^[19].

Zirconium carbide is a technologically useful TMC material for various applications. According to previous studies, the concentration of carbon vacancies in zirconium carbide can be up to 50%^[8-12]. Carbon vacancies are generally disordered in substoichiometric zirconium carbides at high temperatures. After a long-time annealing, these substoichiometric zirconium carbides prefer to adopt ordered carbon vacancies forms^[8,9]. Gusev et al. did some experiments to verify the existence of substoichiometric zirconium carbides with ordered carbon vacancies^[11,12]. According to their experimental studies, Zr_6C_5 , Zr_3C_2 , and Zr_2C are stable, and they also

proposed some ordered structures for these three substoichiometric zirconium carbides based on the order-parameter functional method^[10-12]. However, there remain two unsolved issues: (1) all stable substoichiometric zirconium carbides are not explored; and (2) structures proposed by order-parameter functional method are not always stable. Therefore, a global search for all the stable substoichiometric zirconium carbides is desired.

In the present study, we used the EA method to predict stable substoichiometric zirconium carbides. Based on the predicted structures, we further investigated the effects of carbon vacancies on the structural and mechanical properties of substoichiometric zirconium carbides.

II. Computational Methods

Given only the chemical elements (Zr and C in our case), USPEX can predict all stable compounds and their structures, and here we performed such calculations at zero pressure and zero temperature. Stability of a compound is determined using the thermodynamic convex hull construction. For every candidate structure generated by USPEX, total energy calculations and structure relaxations were carried out using density functional theory (DFT^[20]) within the Perdew-Burke-Ernzerhof generalized gradient approximation (GGA^[21]), as implemented in the VASP code^[22]. The all-electron projector-augmented wave method^[23], with a plane-wave kinetic energy cutoff of 560 eV, and uniform k -point meshes with reciprocal-space resolution of $2\pi \times 0.06 \text{ \AA}^{-1}$, were used. These settings enable excellent convergence of the energy differences, stress tensors, and structural parameters. Denser k -point meshes in reciprocal space with a resolution of $2\pi \times 0.03 \text{ \AA}^{-1}$ were used for detailed calculations of properties.

To ensure the dynamical stability of the predicted compounds, a finite displacement method, as implemented in the PHONOPY code^[24], was used to obtain phonon spectra. For a given crystal, each atom, in turn, is displaced by a small amount, and the forces induced on all the atoms in the crystal are then calculated by VASP and

used to construct the force constant matrix. The VASP calculation is performed on a supercell with a sufficiently large number of atoms. From the force constants matrix we compute the dynamical matrix at any chosen q-point of Brillouin zone, and the diagonalisation of the dynamical matrix provides squares of the phonon frequencies^[24].

The elastic constants, directly related to the mechanical stability of a material, were also calculated by VASP. The mechanical stability criteria for all crystal systems can be found in Ref. 25.

The mechanical properties (bulk modulus B and shear modulus G) of a polycrystalline material, which can be considered to be homogeneous, were evaluated using the Hill averaging scheme^[26-27]. With B and G , the Vickers hardness H_v of a material can be obtained according to Chen's empirical model^[28]:

$$H_v = 2(k^2 G)^{0.585} - 3, \quad (1)$$

where k (equals to G/B) is Pugh's ratio^[29], and all moduli are in GPa.

To relate the mechanical properties with chemical bonding, we have computed the integrated crystal orbital Hamilton populations (ICOHP) using the LOBSTER program^[30-31].

III. Results and Discussions

Results of the global EA search for stable zirconium carbides are shown in Fig. 1. In addition to the most common rocksalt stoichiometric ZrC ($Fm\bar{3}m$) and the previously confirmed substoichiometric Zr_2C ($Fd\bar{3}m$) structures^[8,10,11], our calculations have identified four other stable ordered substoichiometric structures: Zr_8C_7 (space group $P\bar{1}$), Zr_6C_5 ($C2/m$), Zr_5C_4 ($P\bar{1}$), and Zr_3C_2 ($C2/m$). Additionally, the $R\bar{3}m$ phase of Zr_8C_5 possessing the same topology as the stable Ti_8C_5 ^[32] is also discovered. However, the $R\bar{3}m$ phase is metastable as its enthalpy of formation lies above the convex hull. Compared with previous results calculated using the order-parameter functional method by Gusev *et al.*^[10,11] (see Fig. 1), the present EA

search has indentified the same structures for $Fd\bar{3}m$ Zr_2C and $C2/m$ Zr_6C_5 , but has discovered lower-energy structures for Zr_8C_7 ($P\bar{1}$), Zr_3C_2 ($C2/m$), and Zr_4C_3 ($I\bar{4}3m$). Besides, a stable substoichiometric zirconium carbide Zr_5C_4 ($P\bar{1}$) – a composition never reported before – has been found. We have found that this $P\bar{1}$ structure is also adopted by thermodynamically stable Ti_5C_4 and Hf_5C_4 (see Figs. S1&S2 in the Supplementary Material). Detailed structural information for the predicted stable zirconium carbides is listed in Table SI in the Supplementary Material.

To verify the dynamical and mechanical stability of the newly predicted thermodynamically stable substoichiometric zirconium carbides, we have computed phonon dispersion curves and elastic constants for these materials (see Fig. S3 and Table SII in the Supplementary Material). No imaginary phonon frequencies have been found throughout the Brillouin zone, suggesting dynamical stability of these substoichiometric phases. We have also found these substoichiometric zirconium carbides to be mechanically stable because their elastic constants satisfy the mechanical stability criteria^[25].

3.1 Structural properties of stable zirconium carbides

In all of these zirconium carbides, C atoms occupy octahedral voids in the cubic close packing of Zr atoms, and all the C atoms are six-coordinate. In the stoichiometric $Fm\bar{3}m$ ZrC , Zr atoms are six-coordinate, while in substoichiometric zirconium carbides Zr coordination number varies with the number of missing carbon atoms. For stable substoichiometric zirconium carbides Zr_8C_7 ($P\bar{1}$), Zr_6C_5 ($C2/m$), Zr_5C_4 ($P\bar{1}$), Zr_3C_2 ($C2/m$), and Zr_2C ($Fd\bar{3}m$), one-of-eight, -six, -five, -three, and -two octahedral interstitial positions are unoccupied, respectively. As a result, their Zr coordination numbers gradually decrease (see Table SI in the Supplementary Material).

Zr coordination number depicts the information of the carbon vacancy

distribution: if the coordination number of Zr atom is not less than the threshold value five, the carbon vacancies are nonadjacent. If the coordination number of Zr atom is smaller than this threshold value, carbon vacancies near Zr atom will be grouped. Fig. 2(a)-(f) shows different arrangements of carbon vacancies as visualized by the VESTA software^[33]. Carbon vacancies in both $P\bar{1}$ Zr_8C_7 and $C2/m$ Zr_6C_5 are nonadjacent; in fact, Zr_6C_5 is the zirconium carbide with the maximum carbon vacancy concentration that adopts a nonadjacent carbon vacancy structure when all the Zr atoms are five-coordinate. As carbon vacancy concentration increases, the coordination number of Zr becomes smaller than five, and thus carbon vacancies get grouped. As shown in Fig. 2(d)-(f), the stable $P\bar{1}$ Zr_5C_4 phase possesses paired adjacent carbon vacancies. Carbon vacancies are interconnected in $C2/m$ Zr_3C_2 and $Fd\bar{3}m$ Zr_2C .

The evolution of carbon vacancies distribution has an effect on volume of zirconium carbides. The relationships between average volume per Zr atom and the concentration of carbon vacancies are shown in Fig. 2(g). Interestingly, as the concentration of carbon vacancies increases, the volume per Zr atom initially expands and then shrinks. This can be interpreted by the redistribution of bond lengths due to carbon vacancies. As shown in Fig. 3, lattice relaxation around carbon vacancies results in a strongly anisotropic distortion of the structure (see the widely scattered Zr-C and Zr-Zr bonds length in the case of substoichiometric zirconium carbides). In comparison to the bonds length in $Fm\bar{3}m$ ZrC , some Zr-C and Zr-Zr bonds in $P\bar{1}$ Zr_8C_7 and $C2/m$ Zr_6C_5 are shortened (S-bond), while the rest are lengthened (L-bond). With increasing carbon vacancies concentration, more and more carbon vacancies will be grouped, and the lattice relaxation around grouped vacancies will result in shortening of most of bonds (both S-bond and L-bond). Due to this, there is a trend that the number of S-bonds increases while that of L-bonds decreases. These could explain why nonadjacent carbon vacancies can contribute to volume expansion, while the occurrence of adjacent carbon vacancies leads to volume shrinkage.

3.2 Mechanical properties of stable zirconium carbides

The effect of carbon vacancies on mechanical properties (bulk modulus, shear modulus, Pugh's ratio, and Vickers hardness) has also been investigated in this work. The relationships between mechanical properties and the concentration of carbon vacancies are shown in Fig. 4. The bulk modulus and shear modulus vary linearly with the concentration of carbon vacancies, indicating that at a given concentration the distribution of carbon vacancies has a little effect on these moduli. However, the Pugh's ratio first increases and then decreases with increasing carbon vacancies concentration (see Fig. 4). Theoretical Vickers hardness of stable zirconium carbides has been calculated using Eq. (1). Unlike for the bulk and shear moduli, the dependence of hardness on the carbon vacancies concentration is nonlinear and monotonic (see Fig. 4). Just as for the volume, we suppose the distribution of carbon vacancies can affect the Pugh's ratio and hardness of materials. The nonadjacent carbon vacancies enhance Pugh's ratio while the adjacent carbon vacancies decrease Pugh's ratio. The nonadjacent carbon vacancies also have a smaller contribution to the decrease of hardness than adjacent carbon vacancies. To check this hypothesis, Zr_{10}C_9 and Zr_6C_5 structures (denoted by the red squares in Fig. 4) with adjacent carbon vacancies were constructed basing on $P\bar{1}$ Zr_5C_4 and $C2/m$ Zr_3C_2 structures, respectively. In contrast to $P\bar{1}$ Zr_8C_7 with nonadjacent carbon vacancies, $P\bar{1}$ Zr_{10}C_9 has a lower carbon vacancies concentration, but lower Pugh's ratio. $P\bar{1}$ Zr_{10}C_9 is also softer than $P\bar{1}$ Zr_8C_7 and slightly harder than $P\bar{1}$ Zr_5C_4 with adjacent carbon vacancies. Most obviously, $C2/m$ Zr_6C_5 with adjacent carbon vacancies has lower Pugh's ratio and hardness than $C2/m$ Zr_6C_5 with nonadjacent vacancies. Thus, we can conclude that such unusual changes in Pugh's ratio and hardness are related to the evolution of the carbon vacancies distribution.

Some works suggest that the mechanical properties of carbides are directly related to their chemical bonding^[17,19,34]. Our hypothesis for explaining their bulk and shear moduli is that with increasing concentration of carbon vacancies, Zr-C bonding

weakens. This hypothesis is supported by the computed average ICOHP values for bonding Zr-C in all of the stable zirconium carbides. The ICOHP value of a bond can be as an indicator of the bond strength. The average ICOHP value of Zr-C interactions observed in $P\bar{1}$ Zr₈C₇ (2.37 eV/bond), $C2/m$ Zr₆C₅ (2.41 eV/bond), $P\bar{1}$ Zr₅C₄ (2.37 eV/bond), $C2/m$ Zr₃C₂ (2.40 eV/bond), and $Fd\bar{3}m$ Zr₂C (2.24 eV/bond), are smaller than that of in $Fm\bar{3}m$ ZrC (4.70 eV/bond). Due to this decline in the strength of Zr-C bonds, the bulk modulus and shear modulus in the stable substoichiometric zirconium carbides decrease.

The anomalous Pugh's ratio and hardness can also be explained by ICOHP values. There is an anti-correlation between ICOHP values of metal-metal bonds and Pugh's ratio in pyrite-type transition-metal pernitrides^[35]. We found that such correlation between a specific bond with mechanical properties could be applied here. The Zr-Zr ICOHP values of $P\bar{1}$ Zr₈C₇ (0.58 eV/bond), $C2/m$ Zr₆C₅ (0.59 eV/bond), and $P\bar{1}$ Zr₅C₄ (0.58 eV/bond) are lower than that of $Fm\bar{3}m$ ZrC (0.82 eV/bond). Conversely, ICOHP values of Zr-Zr bond in $C2/m$ Zr₃C₂ (1.30 eV/bond) and $Fd\bar{3}m$ Zr₂C (1.31 eV/bond) are higher than in $Fm\bar{3}m$ ZrC. Thus, Pugh's ratio of Zr₈C₇ ($P\bar{1}$), Zr₆C₅ ($C2/m$), and Zr₅C₄ ($P\bar{1}$) are larger than that of $Fm\bar{3}m$ ZrC, while for Zr₃C₂ ($C2/m$) and Zr₂C ($Fd\bar{3}m$) are lower. Thus, Zr-Zr ICOHP values explain the anomalous changes observed in Pugh's ratio and hardness of zirconium carbides.

3.3 A possible way to enhance the hardness of zirconium carbides

As discussed in the previous sections, carbon vacancy can be easily formed in zirconium carbides and the carbon vacancies distribution has a significant effect on the mechanical properties. If small atoms, such as N, B, O, etc, can be easily trapped at vacancy sites (which is thermodynamically favorable at high temperatures), we can expect that an improvement of the mechanical properties of zirconium carbides by replacing carbon vacancies with some suitable atoms. In fact, enhanced hardness has

been reported in transition-metal carbonitrides^[36-38]. That means nitriding substoichiometric zirconium carbides will effectively improve hardness. Here, we have studied the impact of B, N and O on the mechanical properties.

Based on the predicted stable substoichiometric zirconium carbides Zr_8C_7 ($P\bar{1}$), Zr_6C_5 ($C2/m$), and Zr_5C_4 ($P\bar{1}$), we constructed three $\text{ZrC}_{1-x}\text{T}_x$ ($x=1/8, 1/6, 1/5$) structures for each type of element T (T= B, N, O). The relationships between mechanical properties and T content in such compounds $\text{ZrC}_{1-x}\text{T}_x$ were examined (Fig. 4). We can see that only the bulk modulus is improved when doping with B, while enhanced bulk modulus, shear modulus, and hardness are found for doping with N and O. Interestingly, hardness has a maximum in the case of N and O. That means the hardness of some ternary systems can be higher than those of their corresponding binary systems. The valence-electron concentration (VEC^[37,39-41]) can explain the difference between zirconium borocarbides and oxycarbides (or carbonitrides); transition metal nonmetal compounds with the rocksalt structure are expected to have maximum hardness at the same VEC (~ 8.4).

IV. Summary

Evolutionary structure prediction using the USPEX code has been used to solve the controversy regarding the structures and stoichiometries of stable zirconium carbides. In addition to two previously known phases, stoichiometric ZrC ($Fm\bar{3}m$) and substoichiometric Zr_2C ($Fd\bar{3}m$), here we have found four hitherto unknown substoichiometric phases, Zr_8C_7 ($P\bar{1}$), Zr_6C_5 ($C2/m$), Zr_5C_4 ($P\bar{1}$), and Zr_3C_2 ($C2/m$). All of the stable substoichiometric structures have ordered carbon vacancies. The substoichiometric zirconium carbides prefer to adopt structures with nonadjacent vacancy distribution when their carbon vacancy concentration is lower than 1/6. As carbon vacancy concentration increases, the initially nonadjacent carbon vacancies gradually become closer and group together. Such evolution of the distribution of carbon vacancies affects structural and mechanical properties, especially volume,

Pugh's ratio, and hardness. We have studied the mechanical properties of $\text{ZrC}_{1-x}\text{T}_x$ ($x = 1/8, 1/6, \text{ and } 1/5$, and $\text{T} = \text{B}, \text{N}, \text{ and } \text{O}$) constructed by replacing carbon vacancies in $P\bar{1}$ Zr_8C_7 , $C2/m$ Zr_6C_5 , and $P\bar{1}$ Zr_5C_4 with T. An enhanced hardness can be found in the case of N and O. This indicates that nitriding (or oxygen permeating) substoichiometric zirconium (or hafnium) carbides may improve their properties, such as hardness.

Acknowledgements

C. W. Xie thanks Dr. H. Y. Niu for discussing. This work was supported by the Natural Science Foundation of China (Nos. 51372203 and 51332004), the Foreign Talents Introduction and Academic Exchange Program of China (No. B08040), DARPA (Grant No. W31P4Q1210008), and the Government of Russian Federation (Grant No. 14.A12.31.0003). The authors also acknowledge the High Performance Computing Center of NWPU for the allocation of computing time on their machines.

References

- [1] I. Pollini, A. Mosser, J.C. Parlebas, Phys. Rep. 355 (2001) 1-72.
- [2] V.N. Lipatnikov, L.V. Zueva, A.I. Gusev, A. Kottar, Phys. Solid State 40 (1998) 1211-1218.
- [3] V.N. Lipatnikov, A.A. Rempel, A.I. Gusev, Int. J. Refract. Met. H. 15 (1997) 61-64.
- [4] K.E. Tan, A.M. Bratkovsky, R.M. Harris, A.P. Horsfield, D. Nguyen-Manh, D.G. Pettifor, A.P. Sutton, Model. Simul. Mater. SC 5 (1997) 187-198.
- [5] J. Xiang, W. Hu, S. Liu, C. Chen, Y. Zhang, P. Wang, H. Wang, F. Wen, B. Xu, D. Yu, J. He, Y. Tian, Z. Liu, Mater. Chem. Phys. 130 (2011) 352-360.
- [6] P. Wanjara, R.A.L. Drew, J. Root, S. Yue, Acta Mater. 48 (2000) 1443-1450.
- [7] M.M. Opeka, I.G. Talmy, E.J. Wuchina, J.A. Zaykoski, S.J. Causey, J. Eur. Ceram. Soc. 19 (1999) 2405-2414.
- [8] W. Hu, J. Xiang, Y. Zhang, S. Liu, C. Chen, P. Wang, H. Wang, F. Wen, B. Xu, J. He, D. Yu, Y. Tian, Z. Liu, J. Mater. Res. 27 (2012) 1230-1236.

- [9] C.H. De Novion, J.P. Landesman, *Pure Appl. Chem.* 57 (1985) 1391-1402.
- [10] A.I. Gusev, *Phys. Usp.* 43 (2000) 1-37.
- [11] A.A. Rempel, *Phys. Usp.* 39 (1996) 31-56.
- [12] A.I. Gusev, A.A. Rempel, *Phys. Stat Sol. A* 135 (1993) 15-58.
- [13] P.A. Korzhavyi, L.V. Pourovskii, H.W. Hugosson, A.V. Ruban, B. Johansson, *Phys. Rev. Lett.* 88 (2002) 015505.
- [14] J. Billingham, P.S. Bell, M.H. Lewis, *Philos. Mag.* 25 (1972) 661-671.
- [15] A.R. Oganov, C.W. Glass, *J. Chem. Phys.* 124 (2006) 244704.
- [16] C.W. Glass, A.R. Oganov, N. Hansen, *Comp. Phys. Commun.* 175 (2006) 713-720.
- [17] X. Yu, C. R. Weinberger, G. B. Thompson, *Acta Mater.* 80 (2014) 341-349.
- [18] C. Jiang, W. Jiang, *Phys. Stat. Sol. B* 251 (2014) 533-536.
- [19] Q. Zeng, J. Peng, A.R. Oganov, Q. Zhu, C. Xie, X. Zhang, D. Dong, L. Zhang, L. Cheng, *Phys. Rev. B* 88 (2013) 214107.
- [20] W. Kohn, L.J. Sham, *Phys. Rev.* 140 (1965) A1133-A1138.
- [21] J.P. Perdew, K. Burke, M. Ernzerhof, *Phys. Rev. Lett.* 77 (1996) 3865-3868.
- [22] G. Kresse, J. Furthmüller, *Phys. Rev. B* 54 (1996) 11169-11186.
- [23] P.E. Blöchl, *Phys. Rev. B* 50 (1994) 17953-17979.
- [24] D. Alfè, *Comput. Phys. Commun.* 180 (2009) 2622-2633.
- [25] Z. Wu, E. Zhao, H. Xiang, X. Hao, X. Liu, J. Meng, *Phys. Rev. B* 76 (2007) 054115.
- [26] R. Hill, *J. Mech. Phys. Solids* 11 (1963) 357-372.
- [27] R. Hill, *Proc. Phys. Soc. A* 65 (1952) 349-354.
- [28] X. Chen, H. Niu, D. Li, Y. Li, *Intermetallics* 19 (2011) 1275-1281.
- [29] S.F. Pugh, *Philos. Mag. Ser. 45* (1954) 823-843.
- [30] V.L. Deringer, A.L. Tchougreeff, R. Dronskowski, *J. Phys. Chem. A* 115 (2011) 5461-5466.
- [31] S. Maintz, V.L. Deringer, A.L. Tchougreeff, R. Dronskowski, *J. Comput. Chem.* 34 (2013) 2557-2567.
- [32] J.C. Fernandes, C. Anjinho, P.M. Amaral, L.G. Rosa, J. Rodriguez, D. Martinez,

- F.A.C. Oliveira, N. Shohoji, *Mater. Chem. Phys.* 77 (2003) 711-718.
- [33] K. Momma, F. Izumi, *J. Appl. Crystallogr.* 44 (2011) 1272-1276.
- [34] S. Jhi, S.G. Louie, M.L. Cohen, J. Ihm, *Phys. Rev. Lett.* 86 (2001) 3348-3351.
- [35] Z.T.Y. Liu, D. Gall, S.V. Khare, *Phys. Rev. B* 90 (2014) 134102.
- [36] S. Jhi, J. Ihm, S.G. Louie, M.L. Cohen, *Nature* 399 (1999) 132-134.
- [37] M. Holleck, *J. Vac. Sci. Technol. A* 4 (1986) 2661-2669.
- [38] V. Richter, A. Beger, J. Drobniewski, I. Endler, E. Wolf, *Mater. Sci. Eng. A* 209 (1996) 353-357.
- [39] H.W. Hugosson, U. Jansson, B. Johansson, O. Eriksson, *Science* 293 (2001) 2434-2437.
- [40] D.G. Sangiovanni, L. Hultman, V. Chirita, *Acta Mater.* 59 (2011) 2121-2134.
- [41] D.G. Sangiovanni, V. Chirita, L. Hultman, *Thin Solid Films* 520 (2012) 4080-4088.

Figure captions

Fig. 1: Thermodynamic convex hull of the Zr-C system. Circles denote the results of this study; squares indicate calculations by Gusev et al.

Fig. 2: (a)-(f) Atomic arrangement of stable zirconium carbides (ZrC , Zr_8C_7 , Zr_6C_5 , Zr_5C_4 , Zr_3C_2 , and Zr_2C). Green spheres denote Zr atoms; brown spheres, C atoms; squares, carbon vacancies. (g) Relationships between the carbon vacancy concentration and volume per Zr atom (in \AA^3) for all stable zirconium carbides.

Fig. 3: Distribution of Zr-Zr and Zr-C bonds length (in \AA) in stable zirconium carbides (ZrC , Zr_8C_7 , Zr_6C_5 , Zr_5C_4 , Zr_3C_2 , and Zr_2C).

Fig.4: Mechanical properties (bulk modulus, shear modulus, Pugh's ratio and Vickers hardness) of ZrC_{1-x} (x is the concentration of carbon vacancy; $x=0, 1/10, 1/8, 1/6, 1/5, 1/3$, and $1/2$) and $\text{ZrC}_{1-x}\text{T}_x$ ($\text{T}=\text{B, N, and O}$; $x=0, 1/8, 1/6$, and $1/5$) compounds.

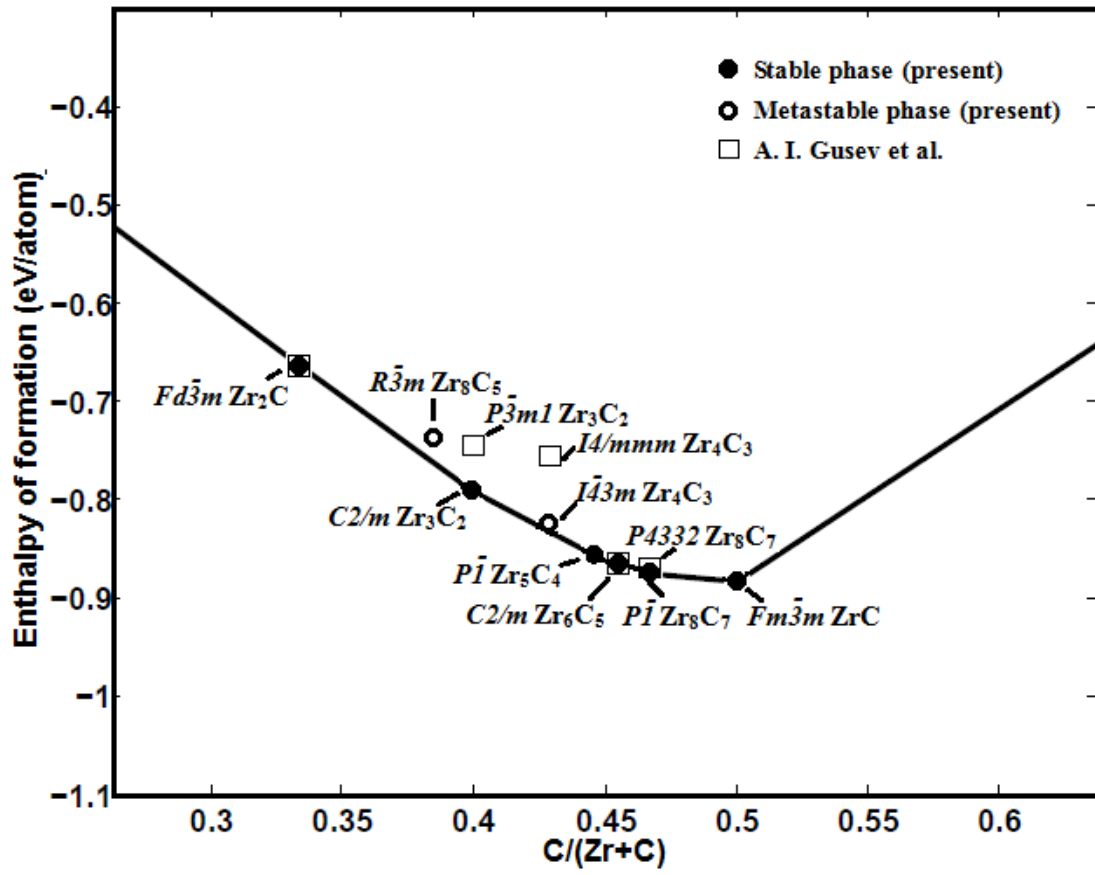


Fig. 1: Thermodynamic convex hull of the Zr-C system. Circles denote the results of this study; squares indicate calculations by Gusev et al.

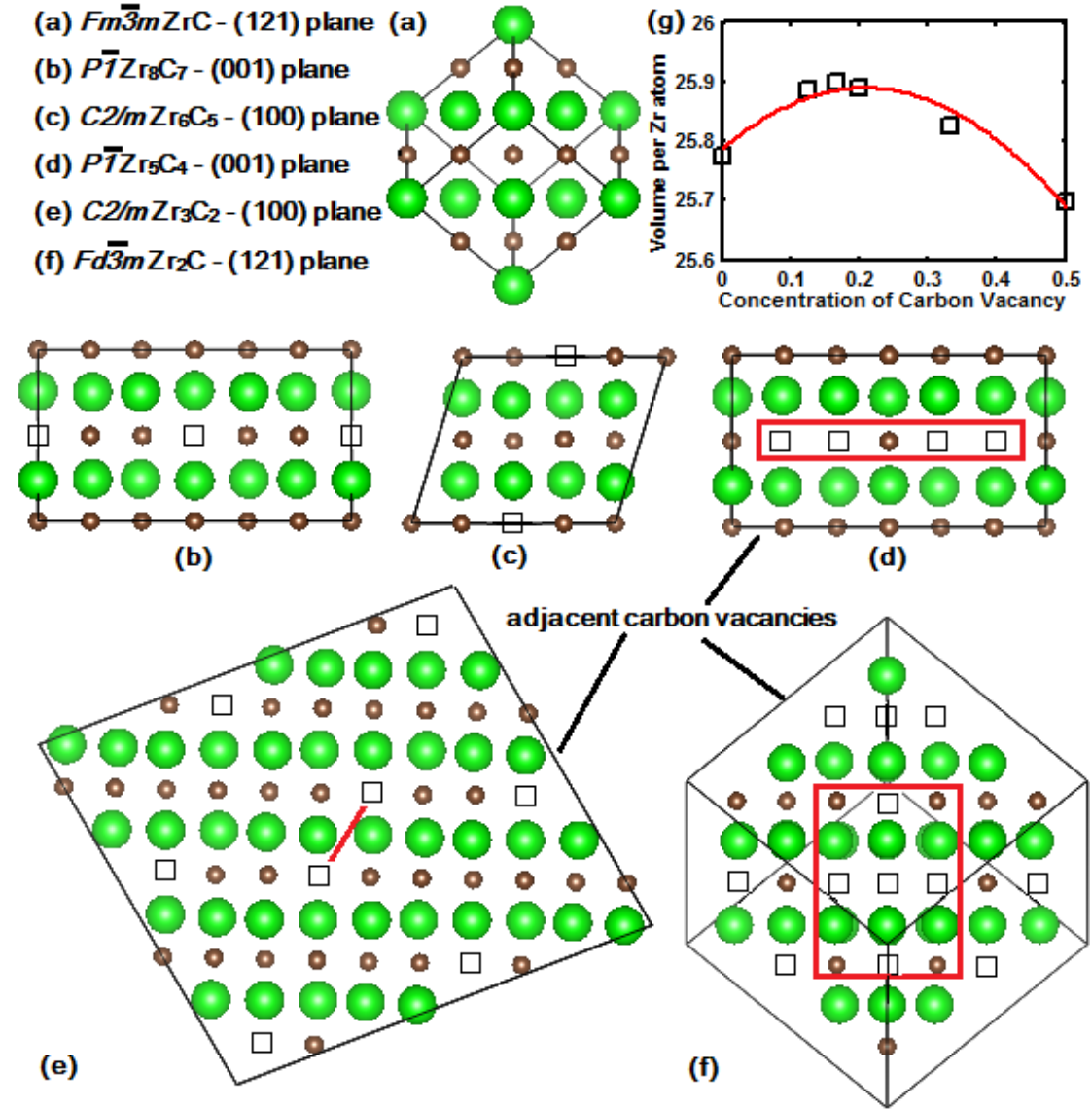


Fig. 2: (a)-(f) Atomic arrangement of stable zirconium carbides (ZrC, Zr₈C₇, Zr₆C₅, Zr₅C₄, Zr₃C₂, and Zr₂C). Green spheres denote Zr atoms; brown spheres, C atoms; squares, carbon vacancies. (g) Relationships between the carbon vacancy concentration and volume per Zr atom (in Å³) for all stable zirconium carbides.

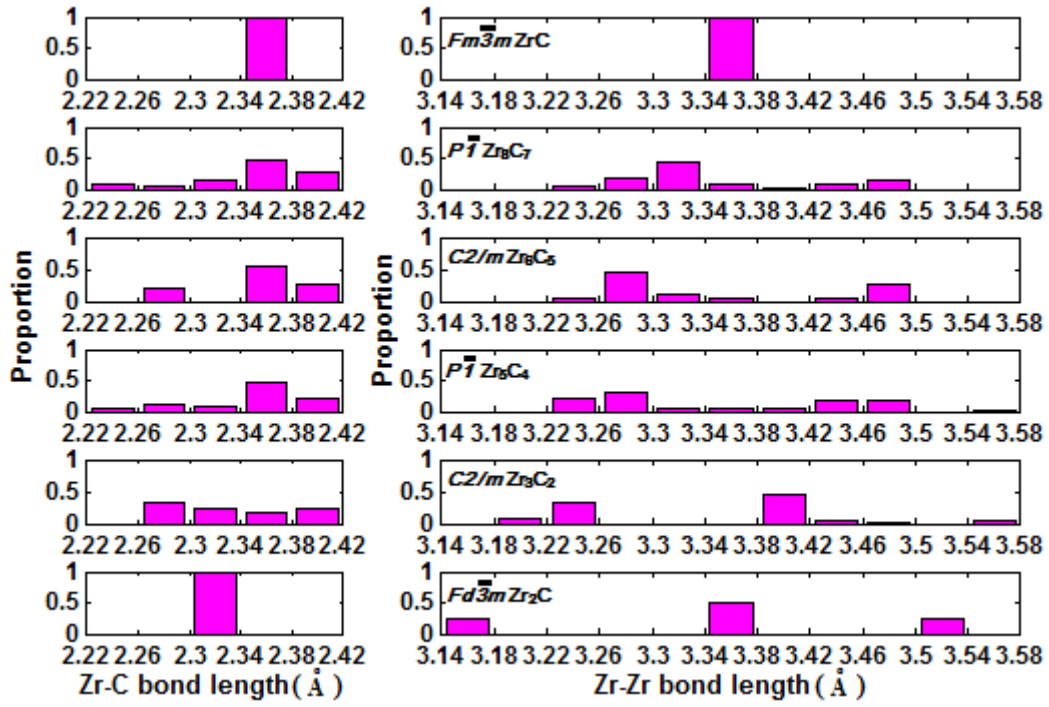


Fig. 3: Distribution of Zr-Zr and Zr-C bonds length (in Å) in stable zirconium carbides (ZrC, Zr₈C₇, Zr₆C₅, Zr₅C₄, Zr₃C₂, and Zr₂C).

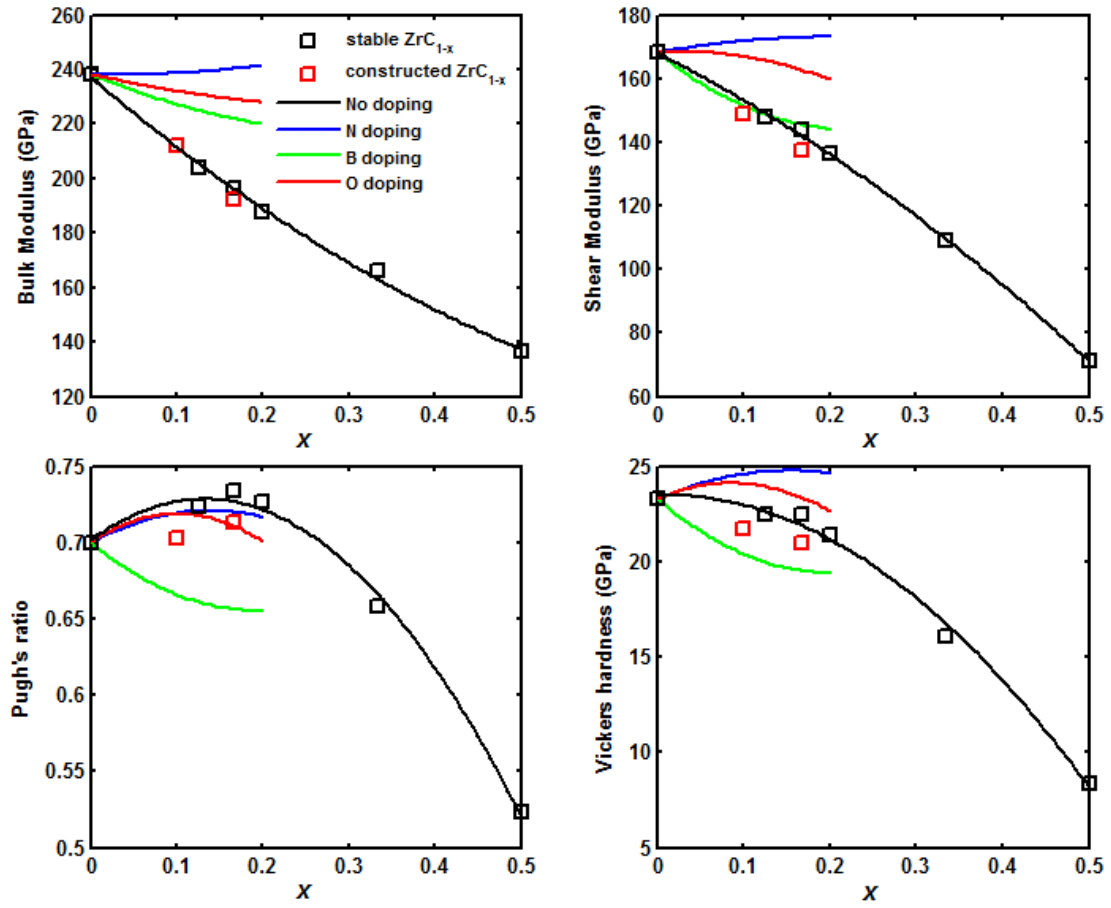


Fig.4: Mechanical properties (bulk modulus, shear modulus, Pugh's ratio and Vickers hardness) of ZrC_{1-x} (x is the concentration of carbon vacancies; $x=0, 1/10, 1/8, 1/6, 1/5, 1/3$, and $1/2$) and $\text{ZrC}_{1-x}\text{T}_x$ ($\text{T}=\text{B}, \text{N}$, and O ; $x=0, 1/8, 1/6$, and $1/5$) compounds.

Supplementary Material

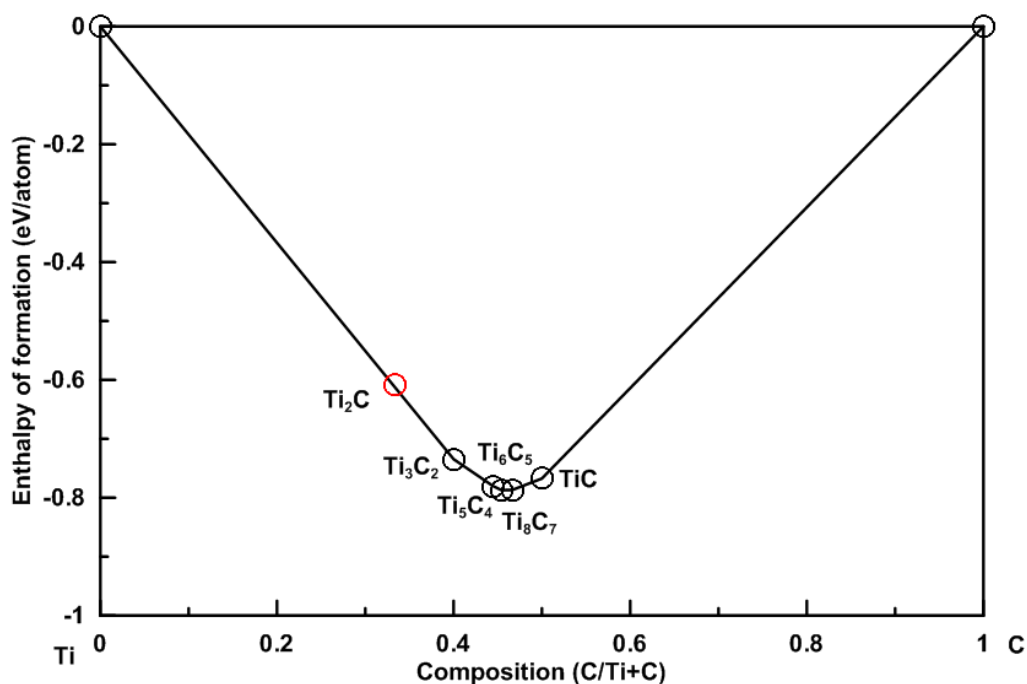


Fig. S1: The thermodynamic convex hull of Ti-C system. Black circles denote the stable phases, while red circle the metastable phase.

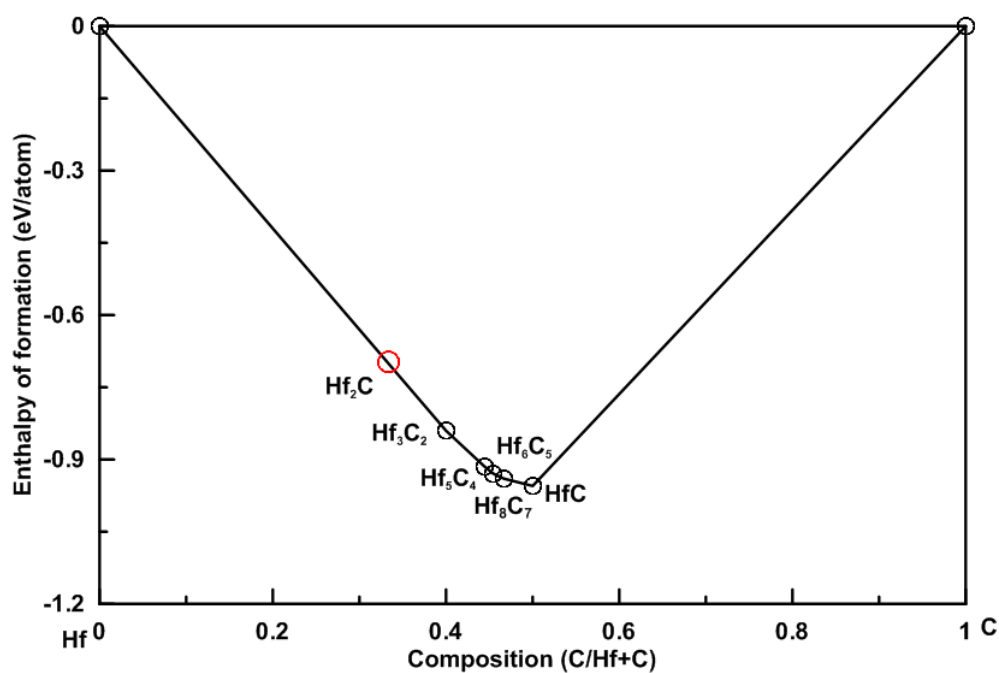
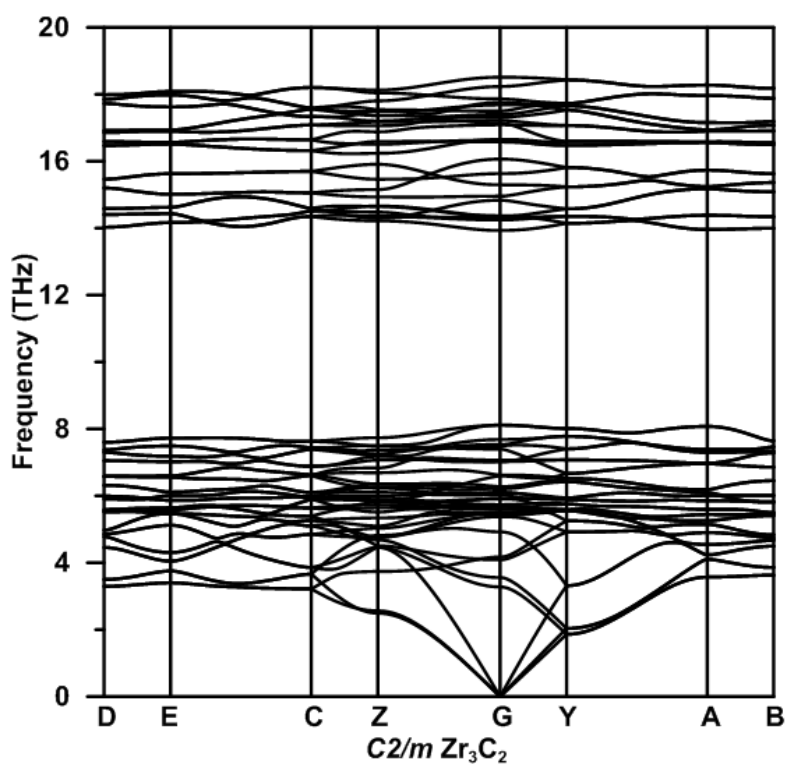
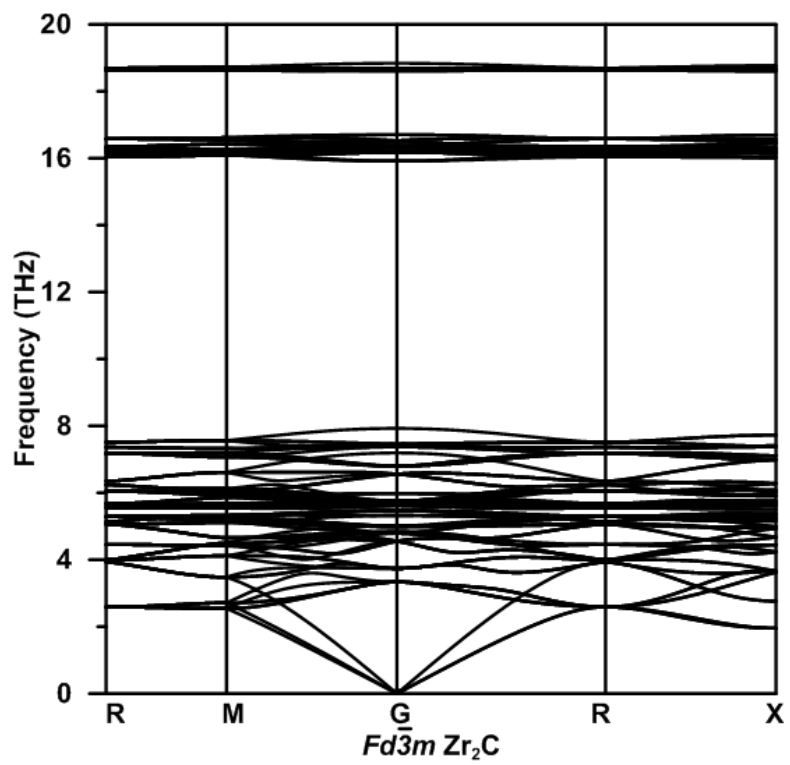
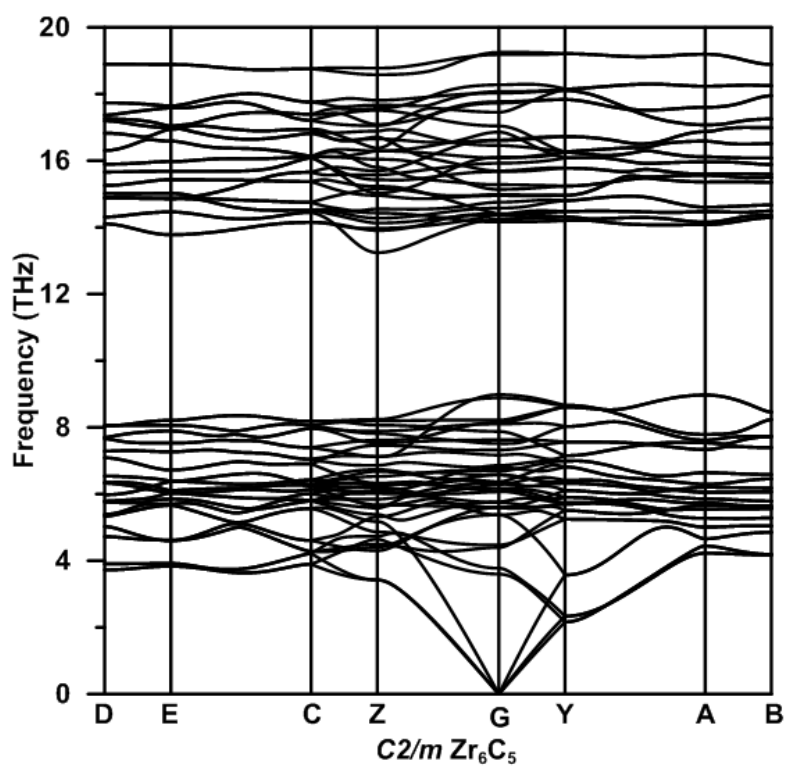
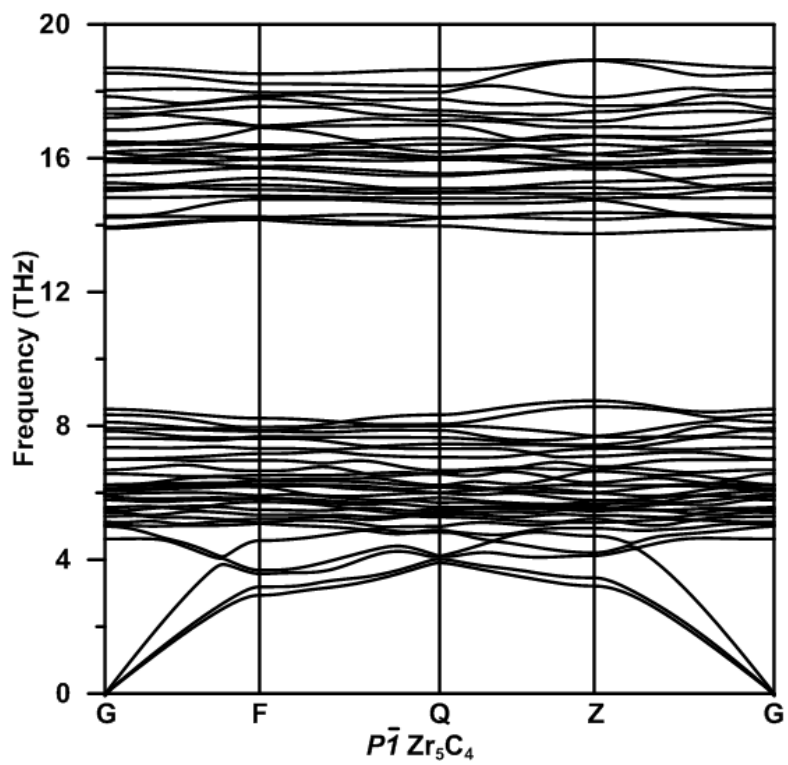


Fig. S2: The thermodynamic convex hull of Hf-C system. Black circles denote the stable phases, while red circle the metastable phase.





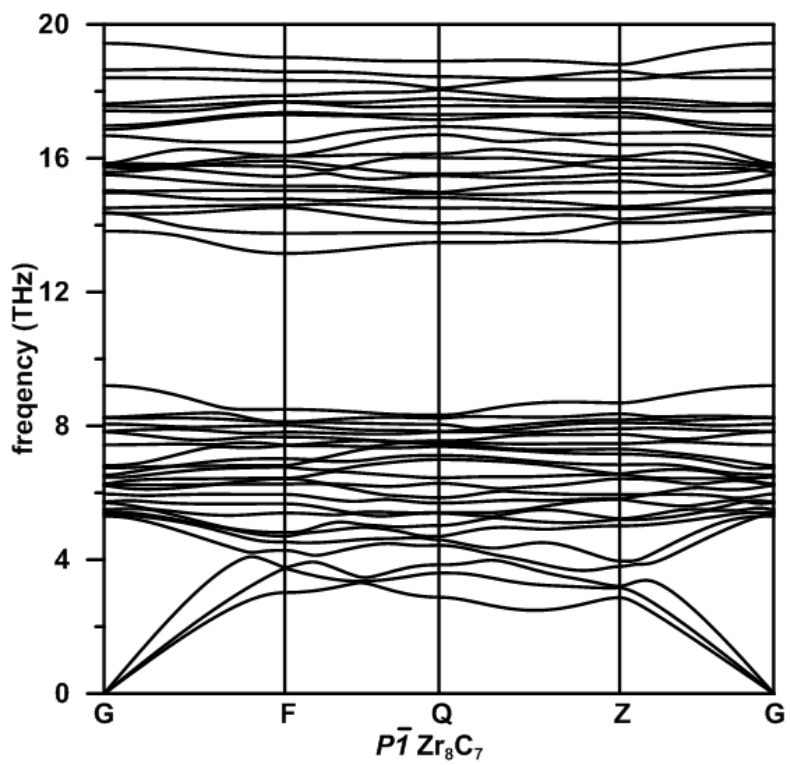


Fig. S3: Phonon dispersion curves computed for all the stable substoichiometric zirconium carbides

Table SI. Geometric details of stable zirconium carbides

ZrC: $Fm-3m$, $a = 4.689$, $V = 103.12$						
Element Symbol	No.	Wyckoff positions	x	y	Z	Coordination Number
C	1	$4b$	0.5	0.5	0.5	6
Zr	1	$4a$	0	0	0	6
Zr ₈ C ₇ : $P-1$, $a = 5.789$, $b = 5.796$, $c = 6.701$, $\alpha = 106.90$, $\beta = 89.93$, $\gamma = 99.34$, $V = 212.01$						
Element Symbol	No.	Wyckoff Positions	x	y	z	Coordination Number
C	1	$2i$	0.2536	0.4976	0.1251	6
C	2	$2i$	0.2488	0.4948	0.6235	6
C	3	$2i$	0.0008	0.9996	0.7476	6
C	4	$1d$	0.5	0	0	6
Zr	1	$2i$	0.3725	0.2624	0.3062	5
Zr	2	$2i$	0.8929	0.2555	0.5653	5
Zr	3	$2i$	0.3706	0.2550	0.8234	5
Zr	4	$2i$	0.8706	0.2454	0.0608	6
Zr ₆ C ₅ : $C2/m$, $a = 5.754$, $b = 9.961$, $c = 6.634$, $\beta = 125.17$, $V = 310.81$						
Element Symbol	No.	Wyckoff Positions	X	y	z	Coordination Number
C	1	$4h$	0.5	0.3340	0.5	6
C	2	$4g$	0.5	0.3317	0	6
C	3	$2b$	0.5	0	0	6
Zr	1	$8i$	0.4954	0.8268	0.7539	5
Zr	2	$4i$	0.9792	0	0.2393	5
Zr ₅ C ₄ : $P-1$, $a = 7.487$, $b = 6.684$, $c = 5.790$, $\alpha = 106.78$, $\beta = 75.07$, $\gamma = 102.84$, $V = 264.62$						
Element Symbol	No.	Wyckoff Positions	x	y	z	Coordination Number
C	1	$2i$	0.7994	0.3482	0.0983	6
C	2	$2i$	0.3995	0.5501	0.3020	6

C	3	$2i$	0.6038	0.9507	0.6996	6
C	4	$2i$	0.0015	0.7523	0.4965	6
Zr	1	$2i$	0.3026	0.3559	0.5873	5
Zr	2	$2i$	0.3057	0.8402	0.5906	5
Zr	3	$2i$	0.5127	0.2560	0.0039	5
Zr	4	$2i$	0.9074	0.5424	0.7940	5
Zr	5	$2i$	0.1081	0.9501	0.2140	4
Zr_3C_2 : $C2/m$, $a = 5.754$, $b = 9.943$, $c = 6.624$, $\beta = 125.17$, $V = 309.80$						
Element Symbol	No.	Wyckoff Positions	x	y	z	Coordination Number
C	1	$2a$	0	0	0.5	6
C	2	$2a$	0	0	0	6
C	3	$4g$	0.5	0.1662	0	6
Zr	1	$8i$	0.5167	0.3391	0.7644	4
Zr	2	$4i$	0.5066	0	0.2439	4
Zr_2C : $Fd-3m$, $a = 9.369$, $V = 822.31$						
Element Symbol	No.	Wyckoff Positions	x	y	z	Coordination Number
C	1	$16d$	0.1250	0.1250	0.6250	6
Zr	1	$32e$	0.3809	0.6191	0.6191	3

Table SII The calculated elastic constants C_{ij} , bulk modulus B (GPa), shear modulus G (GPa), Pugh's ratio and Vickers hardness H_v (GPa) of Zr-C compounds at ambient conditions.

compounds	Zr ₂ C	Zr ₃ C ₂	Zr ₅ C ₄	Zr ₆ C ₅	Zr ₈ C ₇	ZrC
C_{11}	200	312	369	419	395	496
C_{12}	105	88	92	83	110	109
C_{13}		97	101	87	104	
C_{14}			7		17	
C_{15}		-9	7	3	4	
C_{16}			9		7	
C_{22}		331	375	386	397	
C_{23}		86	105	115	106	
C_{24}			6		-6	
C_{25}		-1	-9	-1	5	
C_{26}			-5		-7	
C_{33}		311	353	393	406	
C_{34}			-3		-11	
C_{35}		-3	-5	6	-14	
C_{36}			1		10	
C_{44}	93	110	135	127	156	151
C_{45}			9		4	
C_{46}		-6	-9	-1	9	
C_{55}		96	142	162	148	
C_{56}			-0.2		-9	
C_{66}		114	142	131	146	
B	137	166	188	196	204	238
G	71	109	136	144	148	168
k	0.523	0.658	0.726	0.734	0.724	0.700
H_v	8.4	16.1	21.4	22.5	22.5	23.3